Dynamic behaviour of dry and water-saturated sand under planar shock conditions

M. Arlery, M. Gardou, J.M. Fleureau, C. Mariotti

Accepted Manuscript

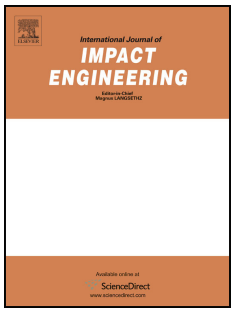

Title: Dynamic behaviour of dry and water-saturated sand under planar shock conditions

Authors: M. Arlery, M. Gardou, J.M. Fleureau, C. Mariotti

PII: S0734-743X(09)00140-7

DOI: 10.1016/j.ijimpeng.2009.07.009

Reference: IE 1819

To appear in: *International Journal of Impact Engineering*

Received Date: 11 September 2008

Revised Date: 20 July 2009

Accepted Date: 29 July 2009

Please cite this article as: Arlery M, Gardou M, Fleureau JM, Mariotti C. Dynamic behaviour of dry and water-saturated sand under planar shock conditions, International Journal of Impact Engineering (2009), doi: 10.1016/j.ijimpeng.2009.07.009

Dynamic behaviour of dry and water-saturated sand under planar shock conditions

M. Arlery*[(1)], M. Gardou[(2)], J.M. Fleureau[(3)] and C. Mariotti[(1)]

[(1)] *Commissariat à l'Energie Atomique, Centre DAM - Ile de France, Bruyères le Châtel, 91297 Arpajon, France*

[(2)] *Direction Générale de l'Armement, Centre d'Etudes de Gramat, 46500 Gramat, France*

[(3)] *Ecole Centrale Paris, Laboratoire MSS-MAT, CNRS UMR 8579, 92295 Châtenay-Malabry, France*

* Corresponding author. Tel. +33-169-26-51-00; Fax. +33-169-26-70-23; E-mail. magali.arlery@cea.fr

Abstract

Plane shock wave experiments were performed on dry and partially water-saturated sand, using three water contents, in order to validate predictive models of material behaviour at stress levels between 1 and 10 GPa. Gas and powder guns were used to load the sample under uni-axial strain conditions at low and high stress levels, respectively. Wave motions were detected by piezoelectric pins in the samples and a VISAR (Velocity Interferometer System for Any Reflector) recorded the free surface velocity on the back target. This study presents both experimental and simulated results. Experimental data are used to determine shock Hugoniot states. Significant differences are observed in the dynamic response of the materials under various water-saturated conditions, and are reproduced with good agreement by numerical simulations using the ARMORS (A Rheological MOdel of Rocks Saturated) model.

Keywords: sand, water-saturation, plate impact, shock Hugoniot, numerical simulation

1. INTRODUCTION

There is a great interest in understanding and modelling the behaviour of geological materials under dynamic loadings such as strong seismic motions, blast wave propagation or impacts. For porous materials like sand, water-saturation may have a significant influence on the soil behaviour. Under such conditions, the models constructed for numerical simulations must adequately describe water incorporation, while the capacity of these models must be validated for a large range of dynamic loading conditions, soils and water contents.

Plane impacts associated with stress gauge measurements are mainly used to characterize shock-wave equation of state and release behaviour of porous materials under dynamic loading. Experimental data established on the dynamic behaviour of sand can compare favourably [1] [2] [3] or with a larger scatter [4]. In the last case, differences are attributed to the wide variety of grain sizes and chemical compositions displayed by this material and/or the difficulties in testing granular materials, especially with gauge assemblies [3] [5] [6].

More limited studies are concerned with water-saturated geologic materials [8] to [12] and especially sands [1] [6] [7]. Experimental results from [7] on dry, 10%, 20% and 23% water saturated samples showed that less than 10% water saturation has little effect in the shock regime, whereas small changes in the water content become significant in the region of 20% water saturation. These results compare well with the results from [1] obtained on dry and 23% and 28% water-saturated sands.

Some of these studies tested models to predict the behaviour of dry and hydrated sand. The calibrated P-λ model used by [4] simulated Hugoniot data of dry sand in a partial compaction regime up to 2 GPa. In [1], experimental shocks adiabats in the 1 to 12 GPa pressure range of different grain-size sands with water-saturations of 23% and 28% were reproduced with 9%

accuracy by calculations using a model of a two interpenetrating deformable continuous media. In [6], the two-phase model used could successfully describe stress gauge histories of dry and hydrated sand in the 1 to 20 GPa stress range.

In this paper, we first investigate the dynamic behaviour of dry sand as well as 53% and 87% water-saturated sand samples at stress level between 1 and 10 GPa, using planar impact experiments on two complementary gun facilities. These experiments were equipped with rarely used both piezoelectric pins inserted in the samples and VISAR rear face recording, allowing the characterization of a shock and a re-shock state for each shot. A special process has been developed to prepare the samples with the highest possible water saturation (87%).

The ability of the ARMORS (A Rheological MOdel of Rocks Saturated) model to reproduce the experiments is secondly assessed. This Lagrangian model has been developed to describe the behaviour of porous and fragile geomaterials with water incorporation and already successfully validated on small–scale explosions in 60% and 80% water-saturated tuff [13].

2. EXPERIMENTAL PROCEDURE

2.1 Material properties

The material investigated is composed of 90% by weight sand and 10% kaolinite, the presence of clay being intended to stabilize and homogenize the water content in the wet samples.

This geologic sand is extracted near Catus, in the department of Lot, southwest of France. It is a quartz sand with a chemical composition about 95% of silica in mass. Detailed chemical composition of this material is given in appendix 1.

Fig. 1a shows a picture of the material before experiment and Fig. 1b reports the grain-size distributions of the sand, clay and mixture, determined according to french standardization organization AFNOR (for «Association Française de NORmalisation») standards NF P 94-056 03/96 [14] and NF P 94-057 05/92 [15].

Table 1 presents the grain-size distribution parameters, as well as the minimum ρ_{0dmin} and maximum ρ_{0dmax} specific densities of the materials, and the specific density of the solids ρ_{0g}. Densities of materials and solids are determined according to AFNOR standard NF P 94-059 [16] and NF P 94-054 [17], respectively. As shown in Table 1 by the increase in the maximum density values of the mixture, the addition of the small percentage of clay increases the compactibility of the mixture,

The definition of all grain-size distribution and material parameters is given in appendix 2.

2.2 Sample preparation

Samples are contained in 5 mm-thick cylindrical cups made of copper (see Fig. 2). This material was chosen for its well-known shock properties. Inside the cup, the sample dimensions are approximately 100 mm in diameter and 15 mm in thickness.

Preliminary compaction tests were performed to determine the optimal initial density of the dry mixture in the cups ρ_{0d} at the three selected degrees of saturation: 0, medium- and nearly-saturated. A mean value of 1.73 g/cm^3 was adopted as the best compromise between two requirements: (i) being relatively easy to obtain with the available loading devices and (ii)

being high enough to ensure that, once in the cups, the soil will be stable and its density will remain constant during transport and handling. The corresponding initial porosity n_0, given by the ratio between void and dry mixture volumes, is equal to 33.8%.

Five samples were prepared, with the same initial dry density ρ_{0d} of 1.73 g/cm^3, water contents w, degrees of saturation S_{0w} and wet densities ρ_0 detailed in Table 2.

The dry samples were directly compacted from dry powder in the moulds. The compacting device, designed to ensure regularity and homogeneity of compaction in the cup, consists of a cylinder fixed on the cup and a piston (Fig. 2). The cylinder has three functions: (i) to reinforce the lateral wall of the cup, which is subjected to a large stress during compaction estimated at 4 MPa, (ii) to hold the soil powder before compaction, (iii) to guide the piston. Compaction is carried out by submitting the soil mixture to an increasing load until its volume is equal to that of the cup, the mass of soil corresponding exactly to the dry density that needs to be obtained. A constant speed loading frame is used to apply the compression force to the piston, first under monotonic conditions up to 60 kN, then with several cycles between 30 and 60 kN. Applying cycles helps reduce the rebound of the piston during unloading.

For the partially water saturated samples, dry powder was mixed with water to a water content of 10.3% which remained constant during compression, as no drainage occurred.

In the case of the nearly saturated sample, the powder was compacted at an initial water content of approximately 15% in order to avoid drainage during compression. After immersion in water for one week, the water content increased to 17.1% and the degree of saturation, to 0.874. The sand experiences no swelling when immersed in water and the kaolinite, very little, most of it taking place during the initial mixing and compression of the specimens.

The cup is finally closed by a rear plate made of copper, fixed in position with a bi-component epoxy glue.

2.3 Plate impact details

Plate impact experiments were performed at the Centre d'Etudes de Gramat, using two complementary gun facilities, to obtain stress levels ranging from 1 to 10 GPa. The lower stress level was produced using the DEMETER gas gun with a bore diameter of 110 mm and an impact velocity close to 500 m/s, and the upper stress level was produced using the ARES powder gun with a bore diameter of 98 mm and an impact velocity close to 850 m/s.

Fig. 3 shows the plate configuration just before impact. The geometry of target and projectile, restricted by the bore diameter of 98 mm, was investigated by pre-test numerical analysis to prevent release wave effects during experimental data acquisition. The projectile consists of a 30 mm-thick copper plate, mounted on the front of an aluminium sabot. The target consists of the copper cup, inner sample and rear copper plate that are 5 mm, 15 mm and 5 mm thick, respectively, in the impact direction. The impact arises at the external surface of the cup base.

The two guns are equipped with impact diagnostic tools: impact velocity, trigger and tilt pins. Impact velocities were measured with a sequential set of shorting pins mounted at the end of the barrel with an accuracy of ± 1%. In these experiments, the target device was aligned to an accuracy below 1 mrad, using incident and reflected laser light in order to allow a highly planar impact.

Piezoelectric pins are used to detect shock wave arrivals at different positions in the sample. These pins are inserted after sample preparation through holes cut perpendicularly to the rear plate. These pins (TME type CA-1135) function from a few 1 kPa up to 200 MPa with a response time of 10 ns. They are 1.6 mm in diameter and 28.7 mm long, three of them being in contact with the internal surface of the cup base every 120° on a diameter of 80 mm. These three pins are used to determine the shock arrival time at the front sample surface. The six other pins are inserted every 60° on a diameter of 25 mm at three different positions in the sample: 3.75 mm, 7.5 mm and 11.25 mm from the cup base. The exact position of these pins is determined by measuring their total length to a precision of ± 0.05 mm before introducing them into the sample and subtracting the length measured beyond the rear plate after insertion. These six pins provide the shock wave arrival time in the sample. The diametrical positions of the pins are chosen according to a pre-test numerical analysis so that useful recorded shock arrivals are unaffected by releases coming from lateral surfaces of the target.

A VISAR (Velocity Interferometer System for Any Reflector) system is used in all the experiments to measure particle velocity u_p on the back surface of the rear plate. This accurate and fundamental measurement tool collects laser light reflected from the back surface of the impulsively loaded target. As the surface moves, the frequency of the reflected light varies in proportion to the changing surface velocity. The VISAR creates interference fringes in number proportional to the surface velocity [18]. For adequate reflectivity, the surface is polished with roughness coefficient $R_a = 0.05$ μm on a central $\Phi = 20$ mm disk. The VISAR system is characterized by a short time resolution, on the order of 1 ns, and a high accuracy of about 1% or less. The data acquisition requires a high-quality and high-frequency transient recorder. These data are processed by computer analysis to obtain the velocity history.

In the specific case of our experiments, the two longest piezoelectric pins (A and D) inserted in the samples might slightly disturb the flow measured by the VISAR. In fact, when the first shock reaches the top of these pins, a shock is directly propagated into the pin to the central face of the rear surface and a conic shape disturbing flow propagates in the samples. However, these disturbances are both considered as minimal because the pin are predominantly made of soft materials and the amplitude of conic flow has a high geometrical decrease from the top of the pin to the rear surface.

3. NUMERICAL SIMULATION

Simulations are performed in 1D planar and 2D axi-symmetric Lagrangian mode with an hydrocode of the Commissariat à l'Energie Atomique. Samples are modelled with the ARMORS model described below. Projectile, cup and rear plate are modelled with a Mie-Gruneisen equation of state, with initial density ρ_{0Cu} and sound velocity c_{0Cu} respectively equal to 8.93 g/cm^3 and 3940 m/s, a Steinberg-Cochran-Guinan elastoplastic constitutive law detailed with copper parameters in [23] and a spall condition based on the tensile stress limit Σ_{Cu} equal to -1.2 GPa.

At the initial time, the projectile is in contact with the target. Square mesh size within the sample is 0.2 mm.

3.1 Dry ARMOR model

ARMOR (A Rheological MOdel for Rocks) was used to model dry samples as brittle elastic-plastic materials with initial porosity. General outline of the model is given here, but a detailed description can be found in [19].

In this Lagrangian model, isotropic and deviatoric behaviours are coupled by means of a scalar damage variable *D*.

Isotropic behaviour is modelled by a relation between the material density ρ and the hydrostatic pressure *P*. As shown in Fig. 4a, it is defined within a region $\mathcal{D}$ bounded by the elastic part of the isotropic compression path for the porous material, the high-pressure isotropic compaction curve for grains, the extreme unloading and tension limit (taken equal to zero in the particular case of sand, as this material is considered to have no tension resistance). Intermediate loading-unloading curves can be interpolated with a calculation based on regular meshing of inner domain $\mathcal{D}$. The elastic path, limited to pressures less than P_{EL}, is characterized by initial density ρ_0, sound velocity c_0 and compressibility modulus $K_0 = \rho_0 c_0^2$. Pressures greater than P_{EL} induce compaction with a progressive increase in stiffness. At higher pressure, the compaction path joins the compaction path for grains, and there is no significant change in stiffness. Unloading from this path intersects the density axis at grain specific density ρ_{0g}. Hydrostatic tensile stress is limited by the P_{TL} value.

Deviatoric behaviour is defined in the (*P*, *q*) plane, where the variable q is the Von Mises stress, measuring the intensity of the deviatoric component *s* of the stress tensor according to Eq. 1. As shown in Fig. 4b, this domain is made up of a brittle and a ductile region, separated by a transition pressure P_t. In the brittle region, yield curve *S* is a function of the damage level *D,* whereas all yield curves in the ductile region merge to form a single curve.

$$q^2 = \frac{3}{2} s_{ij}^2 \qquad (1)$$

3.2 Water saturated ARMORS model

For partially water saturated materials, a numerical approach has been developed to couple the ARMOR model for dry materials with a Mie-Gruneisen equation of state for water taken form [22]. This model, known as ARMORS (for ARMOR Saturated), is described in detail

and validated with good accuracy in [13] using partially saturated Hudson Moon Tuff subjected to a spherical explosive. In this model, the constitutive law for dry material is unchanged but written in terms of effective stresses, while a purely isotropic mechanism is added to determine the pressure of the water-grain mixture. The approach is based on the assumption that the deviatoric behaviour of the dry material is not modified by water and that the grain and water pressures are equal. The isotropic compressive law for the grains is defined by the upper part of the isotropic compressive curve and the extreme release according to the dry porous ARMOR law.

3.3 Actual dry material parameters

Table 3 summarizes the main parameters of the ARMOR model used to describe the dry samples. These parameters were defined as follows.

In the 1 to10 GPa pressure range, material constants of the isotropic law are determined to fit experimental velocity profiles of shots DM1 and AR1. Below this pressure range, the domain is extrapolated using data of similar sand materials [20], for which bulk modulus K_0 is 200 MPa and elastic pressure limit P_{EL} is 5 MPa. As previously justified, the tension limit is taken as equal to zero. Above the 1 to 10 GPa pressure range, the isotropic law is described by quartz data from [21]. Extreme unloading is adjusted to fit both the lower part of the quartz curve and the initial grain density measured for the samples (see Table 1).

The deviatoric part of the ARMOR law is described by data of similar sand materials [20], for which initial shear modulus is G_0=100 MPa, transition pressure is P_t=7.5 GPa and maximal yield strength in the ductile domain is Y_{max}=1 MPa. As shown later, this maximum yield strength is much lower than the stress normal to the direction of shock propagation σ_x (1

to 10 GPa) reached in the samples under all five plate-impact experiments. Therefore, σ_x will be taken as equivalent to hydrostatic pressure P.

4. RESULTS

4.1 Experimental measurements

Plate impact experiments induce a uniaxial strain state with three-axial stress in the materials. At contact interfaces, the particle velocities and stresses are continuous and reflections are governed by differences in impedance $Z_i = \rho_i.c_i$ between materials. In the particular case of weak material such as sand submitted to high stress range, it can be assumed that stress σ_x in the direction of wave propagation is equivalent to hydrostatic pressure P.

As illustrated on the distance vs. time graph of Figs. 5a and pressure vs. particle velocity graph of Fig. 5b, the impact of the projectile onto the target at initial velocity u_0 generates a shock wave, associated with particle velocity $u_0/2$ and pressure P_0, propagating from the impact plane into the projectile as well as the copper cup base plate.

The shock generated by the impact is transmitted at the copper cup/sample interface as a first shock that propagates forward the sample with associated particle velocity u_1 and pressure P_1. At the sample/rear-plate interface, this first shock is reflected as a second shock that propagates both backward into the sample and forward to the rear plate, with associated particle velocity u_2 and pressure P_2.

For each shot, the sample thus undergoes two successive shock events: the first one brings the sand at a shock state (u_1, P_1) lying on the principal Hugoniot and the second one,

associated to a higher pressure, brings the sand at a re-shock state (u_2, P_2) lying on the Hugoniot starting from (u_1, P_1) pole,

When the second shock reaches the rear-plate free surface, a total release occurs that impulsively moves the surface at velocity u_p. This velocity is maintained until a subsequent wave transmitted by the rear-plate/sample interface returns to the free surface; the velocity history is thus characterized by an initial plateau at mean velocity u_p.

Table 4 summarizes impact conditions and associated measured data for all five shots. As all five are done under different conditions (water content and impact velocity), the repeatability of the results could not be tested. However, as this experimental program was limited, the choice was made to obtain different shock conditions for each shot, in order to characterise as many shock conditions as possible..

For each shot, the measured data are:

(i) impact velocity u_0, measured with a sequential set of shorting pins mounted at the end of the cup plate with an accuracy of ± 1%. For both guns, one can notice the good repeatability of impact velocities which allows to obtain comparable initial compression in the samples.

(ii) first shock velocity U_1, derived from linear regression of the position-time pin measurement data. The shock arrival is detected on each of the nine pins distributed at different positions within the sample. Initial time of impact is determined according to the arrival time at (X, Y, Z) pins and the estimated duration of initial shock propagation through the copper cup-plate. This duration is calculated using the measured impact velocity u_0, cup-plate dimensions and Hugoniot properties of copper. Thus, the experimental uncertainty on the value of U_1 depends on measurements of pin position and plate length (± 0.1 mm each), pin response time (± 10 ns) and impact velocity accuracy (± 1%). The uncertainty on the Hugoniot parameters for copper, used to calculate the initial time, proves to be negligible.

(iii) free-surface particle velocity u_p, associated with the second shock total release at the rear free surface. It is defined as the mean value of the initial plateau extracted from VISAR profiles with a 1% precision.

4.2 Shock Hugoniot states

The locus of the possible thermodynamic states attained by shock waves defines the shock Hugoniot of the material. Two shock states can be inferred from our experiments, using the impedance matching relations at boundaries between different materials and the Rankine-Hugoniot relation involving mass, momentum and energy conservation across the shock front. These relations are derived for first and second shocks, respectively, in Eq. (2a) and Eq. (2b), where u_i is the particle velocity, P_i the pressure, U_i the shock velocity and ρ_i the density in samples, respectively under incident shock ($i=0$), first shock ($i=1$) and second shock ($i=2$).

$$\left.\begin{array}{c} \rho_0 \times U_1 = \rho_1 \times (U_1 - u_1) \\ P_1 = \rho_0 \times U_1 \times u_1 \\ u_1^2 \times B_{cu} - u_1 \times (A_{cu} + 2 \times B_{cu} \times u_0 + \dfrac{\rho_0}{\rho_{0cu}} \times U_1) + A_{cu} \times u_0 + B_{cu} \times u_0^2 = 0 \end{array}\right\} \quad (2a)$$

$$\left.\begin{array}{c} \rho_2 \times (U_2 + u_2) = \rho_1 \times (U_2 + u_1) \\ P_2 = \rho_{0cu} \times (A_{cu} + B_{cu} \times u_2) \times u_2 \qquad with \qquad u_2 = \dfrac{u_p}{2} \\ P_2 = \rho_0 \times U_2 \times (2 \times u_1 - u_2) \end{array}\right\} \quad (2b)$$

Eqs. (2) are based on two fundamental hypotheses: (i) uni-axial strain state is assumed until useful experimental data are acquired: this condition was investigated by pre-test numerical analysis and subsequently confirmed on all the shots but one by comparing 1D and

2D simulations with experimental VISAR measurements, (ii) stress in the direction of shock propagation σ_x in the samples is taken as equivalent to hydrostatic pressure P: this approximation is justified by the very small deviatoric effects compared to pressures (1 to 10 GPa) induced by successive shocks in the experiments.

Eqs. 2 can be solved using both material parameters: initial density ρ_{0Cu}, and Hugoniot coefficients A_{Cu} and B_{Cu} of the copper, respectively equal to 8.93 g/cm^3, 3940 m/s and 1.54, and the three experimentally measured values of impact velocity u_0, first shock velocity U_1 and particle velocity u_p (see Table 4).

Fig. 6a shows the results plotted in shock velocity U vs. particle velocity u space. For a given particle velocity, increased shock velocity with water saturation proves the significant effect of water incorporation on the soil behaviour.

In general, shock-compressed solids well above hydrostatic elastic pressure P_{HEL} obey the Eq. 3 linear relation between U and u. For dry samples, the present data approximately fit this linear relation, with A equal to 270 m/s and s equal to 2.6. For 53%-saturated samples, the U - u relation is clearly non-linear and can be approximated as U= 908 + 2.66 × u for u ≤ 750 m/s, and U= 2411 + 1.26 × u for u ≥ 750 m/s.

$$U = A + B \times u \qquad \textit{with A equal 270 and B equal 2.6} \qquad (3)$$

Fig. 6b reports the results plotted in pressure P vs. mixture density ρ space. Isotropic dry and water saturated paths used by numerical simulations are also plotted.

In the 1 to 10 GPa pressure range of the shots, the ARMOR dry isotropic path, determined to fit experimental VISAR profiles of dry samples, passes exactly through the lowest pressure

(1.34 GPa) experimental Hugoniot data point, but lies slightly above the experimental data points at higher pressure range. However, it is noteworthy that these differences are included within experimental uncertainties. Comparison of data with the quartz shock Hugoniot suggests that total compaction should have occurred at pressures above 3.5 GPa as attained during second shocks for shots DM1 and AR1.

The effect of water incorporation is reflected by the increase in stiffness of the compaction path with water saturation. In the 1 to 10 GPa range of the shots, the isotropic behaviour of wet samples thus seems not to be governed by effective pressure of the dry material but by the pressure of the water-grain mixture, according to grain and water mass conservation. However, one can notice that 53% and 87 % saturated samples show much smaller differences in the experimentally measured behaviour than dry and 53% saturation. Indeed, the ARMORS model previsions for 87% saturated samples expected higher stiffness of the compaction path. In fact, the numerical fitting for this sample could be improved with specific parameters, but our purpose is to dispose of a predictive model for all possible saturations, which is only built with data on dry material and water if no data for saturated material are available.

4.3 Comparison of simulated and experimental measurements

Figs. 7a to 7c show piezoelectric pin measurements plotted on a graph of position vs. first-shock arrival time for dry, 53% and 87% water–saturated samples, respectively. Superposed calculated plots are determined by recording pressure histories at Lagrangian markers. Because of mesh space discretization, these markers are located nearly but not exactly at the experimental positions of the pins. Hence, suitable comparisons must be performed on the slope obtained by linear regression on the plots. This slope corresponds directly to the first-

shock velocity U_1 used for determining shock Hugoniot data. On both measured and simulated data, the shock velocity increases with impact velocity and water-saturation. The difference between measured and calculated velocities does not exceed 7% for all shots.

Figs. 8a to 8c show VISAR measurements of particle velocity at the rear plate free surface for dry, 53% and 87% water–saturated samples, respectively. Earlier and higher surface loading is observed with increasing water saturation and initial impact velocity. The calculated velocity profiles are superposed. They are obtained with a Lagrangian marker positioned at the last mesh cell of the rear-plate. For all shots, both 1D-plane and 2D-axisymetric simulations were performed to estimate the arrival time of peripheral release waves in the VISAR acquisition zone. Except for shot DM1, comparison of 1D and 2D calculations with experimental results show that planar 1D wave conditions are maintained at least until the first VISAR velocity plateau is reached. For all shots, experimental and 2D calculated profiles show good agreement on the profile shape even after the first plateau, when 2D wave flow is achieved. The arrival time of the shock on the free surface is reproduced with an accuracy of 4%. The first velocity plateau associated with total release on the free surface is also reproduced with 4% accuracy.

5. CONCLUSION

Planar shock experiments performed with gas and powder guns on dry, 53% and 87% water-saturated sand samples show significant differences in dynamic behaviour of the material according to water content. For each shot, piezoelectric pins and VISAR free-surface velocity measurements allow the determination of two shock Hugoniot states in the pressure range of 1 to 10 GPa. For a given compression, water incorporation increases shock velocity

and pressure in the material. The shock velocity vs. particle velocity relation is approximately linear for dry samples, but distinctly non-linear for 53% water-saturated samples. Comparison of the Hugoniot curve for dry samples with the compaction path of quartz suggests that total compaction occurs in the dry materials at pressures higher than 3.5 GPa. The observed increasing stiffness of compaction paths along with hydration demonstrates the important effect of water incorporation on the dynamic response of porous materials.

Numerical simulations performed with ARMORS model show good agreement with the piezoelectric pin and VISAR measurements for all shots: discrepancies between calculations and experiments do not exceed 7% for shock velocity and 4% for the main characteristics of VISAR velocity profiles in the 1D flow regime. Furthermore, subsequent 2D lateral releases observed on VISAR profiles are also well reproduced by calculations. For all shots, the model only uses a constant set of parameters for the dry material and a Mie-Gruneisen equation of state for water. These results, associated with previous results obtained on tuff under explosive loading [13], give confidence in the capability of the ARMORS model to simulate water incorporation in porous geological materials under dynamic loading.

ACKNOWLEDGMENTS

The experiments were performed at Direction Générale de l'Armement, Centre d'Etudes de Gramat by Pascal Bouinot and Alain Halgand. The data analysis was performed by Pierre-Louis Héreil.

APPENDIX 1: Chemical composition of the sand

Chemical analyses were performed by microprobe for the principal elements and by gravimetry for sulfates, according to French standard NF EN 196-2.

Element	Na_2O	MgO	Al_2O_3	SiO_2	SO_3	Cl	K_2O	CaO	TiO_2	MnO	Fe_2O_3	Fire loss
Mass (%)	0.1	0	1.6	96.4	0.1	0	1.1	0.1	0	0.1	0.1	0.3

APPENDIX 2: Definition of the material parameters

- Grains-size distribution
  - maximum grain diameter : D_{max}
  - diameter D_i , with $0 \leq i \leq 100$ % is the grain diameter for which the weight of particles with diameter lower than D_i is *i*% of total weight.
  - uniformity coefficient C_u : $C_u = \frac{D_{60}}{D_{10}}$
  - curvature coefficient C_z : $C_z = \frac{D_{30}^2}{D_{10} \times D_{60}}$
- Dry materials and samples
  - ρ_{0dmin} and ρ_{0dmax} are specific minimum and maximum densities of the dry materials (sand, clay and mixture); they are determined using AFNOR standard NF P 94-059 by filling a standardized mould with a well defined procedure for ρ_{0dmin} and applying a normalized stress on vibrating conditions for ρ_{0dmax}
  - ρ_{0g} is the specific density of the solid grains (sand and clay) ; it is determined using AFNOR standard NF P 94-054 [15]
  - ρ_{0d} is the initial optimal density of the dry samples (mixture) in the experimental cups ; it is chosen between specific densities ρ_{0dmin} and ρ_{0dmax}, so

that it is relatively easy to obtain with the available loading devices and stable at the three selected water saturations

- Initial porosity n_0 is the ratio of initial void volume V_{0v} to initial dry sample volume V_{0d} in the experimental cups

$$n_0 = \frac{V_{0v}}{V_{0d}} = \left(1 - \frac{\rho_{0d}}{\rho_{0g}}\right)$$

- Water saturated samples
  - initial water saturation S_{0w} is the ratio of water volume V_{0h} to void volume V_{0v}

$$S_{0w} = \frac{V_{0h}}{V_{0v}} = \frac{V_{0h}}{n_0 \times V_{0d}} = \left(\frac{V_{0h}}{V_{0d}}\right) \times \left(\frac{\rho_{0g}}{\left(\rho_{0g} - \rho_{0d}\right)}\right)$$

  - initial wet density ρ_0

$$\rho_0 = \left[\rho_{0d} + S_{0w} \times \rho_{0w} \times \left(1 - \frac{\rho_{0d}}{\rho_{0g}}\right)\right]$$ with ρ_{0w} is initial water density

REFERENCES

1. Dianov, M. D., Zlatin, N. A., Mochalov, S. M., Pugachev, G. S., and Rosomakho, L. K. (1976). Shock compressibility of dry and water-saturated sand, Soviet Technical Physics Letters 2, p. 207-208.

2. Tsembelis K., Proud W. G. , Vaughan B.A.M. and Field J.E.. "The Behaviour of Sand under Shock Wave Loading: Experiments and Simulations. Proceedings of 14th Technical Meeting organized by Association DYMAT 2002, Sevilla, Spain, p. 193-203.

3. Chapman D. J., Tsembelis K., and Proud W. G. The behaviour of dry sand under shock-loading. Shock Compression of Condensed Matter 2005, edited by M. D. Furnish et al., American Institute of Physics, p. 1445-1448.

4. Brown J. L., Vogler T. J., Grady D. E., Reinhart W. D., Chhabildas L. C. and Thornhill T. F. Dynamic compaction of sand. Shock Compression of Condensed Matter 2007, edited by M. Elert et al, American Institute of Physics, p.1363-1366.

5. Resnyansky A. D. and Bourne N. K. Shock-wave compression of a porous material. J. Appl. Phys. 2004; 95. p.1760-1769.

6. Proud W. G., Chapman D. J., Williamson D. M., Tsembelis K., Addiss J., Bragov A. M., Lomunov A., Cullis I. G., Church P. D., Gould P., Porter D., Cogar J. R. and Borg J. P. The dynamic compaction of sand and related porous systems. Shock Compression of Condensed Matter 2007, edited by M. Elert et al, American Institute of Physics, p. 1403-1408.

7. Resnyansky A. D. and Bourne N. K. Shock compression of dry and hydrated sand. Shock Compression of Condensed Matter 2004, edited by M.D. Furnish et al, American Institute of Physics, p. 1474-1477

8. Lomov I. N., Hiltl M., Vorobiev O.Y., Glenn L.A. Dynamic behavior of berea sandstone for dry and water saturated conditions. Int. J. of Impact Eng. 2001;26 p. 465-474.

9. Lysne P. C. A comparison of calculated and measured low-stress Hugoniots and release adiabats of dry and water-saturated tuff. J. of Geophysical Research 1970;75 p. 4375-4386.

10. Erskine D., Nellis W.J., Weir S.T. Shock wave profile study on tuff from the Nevada Test Site. J. of Geophysical Research 1994;99(B8) p.15,529-15,537.

11. Larson D. B., Anderson, G.D. Plane shock wave studies of porous geologic media. J. of Geophysical Research 1979;84(B9) p. 4592-4600.

12. Larson D. B., Anderson, G.D. Plane shock wave studies of westerly granite and nugget sandstone. Int. J. Rock Mech. Min. Sci. & Geomech. Abstr.1979;17 p. 357-363.

13. Mariotti C., Perlat J.P., Guerin J.M. A numerical approach for partially saturated geomaterials under shocks. Int. J. of Impact Eng. 2003;28(7) p. 717-741.

14. AFNOR standard NF P 94-056. Sols : reconnaissance et essais – Analyse granulométrique – Méthode par tamisage sec après lavage. AFNOR March 1996. Can be found in and bought from the following Internet site : http://www.boutique.afnor.org/NEL1AccueilNormeEnLigne.aspx

15. AFNOR standard NF P 94-057. Sols : reconnaissance et essais - Analyse granulométrique des sols - Méthode par sédimentation. AFNOR May 1992. Can be found in and bought from the following Internet site : http://www.boutique.afnor.org/NEL1AccueilNormeEnLigne.aspx

16. AFNOR standard NF P 94-059. Sols : reconnaissance et essais - Détermination des masses volumiques minimale et maximale des sols non cohérents. AFNOR November 2000. Can be found in and bought from the following Internet site : http://www.boutique.afnor.org/NEL1AccueilNormeEnLigne.aspx

17. AFNOR standard NF P 94-054. Sols : reconnaissance et essais - Détermination de la masse volumique des particules solides des sols - Méthode du pycnomètre à eau. AFNOR October 1991. Can be found in and bought from the following Internet site : http://www.boutique.afnor.org/NEL1AccueilNormeEnLigne.aspx

18. Sweatt W.C., Stanton P.L., Crump O.B. Simplified Velocity Interferometer System for Any Reflector (VISAR). Proceedings of Ultrahigh- and High-Speed Photography, Videography, Photonics, and Velocimetry Vol. 1346 1990, edited by P.A. Jaanimagi and al, p.151-159.

19. Mariotti C., Thomas F. Loi de comportement ARMOR pour géomatériaux sous chargement dynamique. Journal de Physique IV 1994; Colloque C8(4) p. 577-582.

20. Stephens D.R. Equation of state of grout and stemming materials. Lawrence Radiation Laboratory, Livermore 1966.

21. Bridgman P. The compression of 39 substances to 100,000 kg/cm^2. Collected Experimental Papers 1947;6 p. 160-3819, Harvard University Press, Boston, Mass.

22. Paplinski A., Wlodarczyk E. An analysis of the equations of state of water from low to very high values of pressure. J. Tec. Phys. 1992;33 p. 363-73

23. Steinberg, D. J., S. G. Cochran, et al. A constitutive model for metals applicable at high strain rate. J. Appl. Phys. 1980;51(3) p. 1498-1504

FIGURE CAPTIONS

Fig. 1. (a) Picture of the dry material. (b) Grain-size distribution of the sand, clay and mixture.

Fig. 2. Sketch diagram of the compaction device.

Fig. 3. Schematic plate impact configuration just before impact. (a) cross-sectional view of projectile and target; (b) view of back of target.

Fig. 4. ARMOR model for dry material. (a) isotropic behaviour; (b) deviatoric behaviour.

Fig. 5. Schematic wave paths of the experiments: shock curves are indicated in solid lines and release in dashed lines). (a) distance from impact plane versus time from impact; (b) pressure P versus particle velocity u.

Fig. 6. Hugoniot data for dry, 53% and 87% water-saturated samples. (a) shock velocity U versus particle velocity u; (b) pressure P versus sample density ρ.

Fig. 7. Distance of gauge from sample/base plate interface versus arrival time of first shock : mean slope gives the velocity of the shock. Experimental data in solid lines and calculated data in dashed lines. (a) dry samples, shots AR1 and DM1; (b) 53% water-saturated samples, shots DM2 and AR2; (c) 87% water-saturated sample, shot AR3.

Fig. 8. Velocity histories of free rear surface measured by VISAR (bold solid lines) and calculated for either 1D planar (dashed lines) or 2D axi-symmetric (solid lines) conditions. (a)

dry samples, shots DM1 and AR1; (b) 53% water-saturated samples, shots DM2 and AR2; (c) 87% water-saturated sample, shot AR3.

Table 1

Parameters of the sand, clay and mixture.

Material	D_{max} **(mm)**	**< 80 µm (%)**	**Uniformity coefficient** $C_U = D_{60}/D_{10}$	**Curvature coefficient** $Cz=D_{30}^2/D_{60}.D_{10}$	ρ_{dmin} **(g/cm^3)**	ρ_{dmax} **(g/cm^3)**	ρ_g **(g/cm^3)**
Sand	1.0	3.0	3.2	1.2	1.360	1.688	2.609
Clay	0.03	100	13	0.56	-	-	2.650
Mixture	1.0	12	18	5.8	1.360	1.856	2.613

Table 2

Characteristics of the prepared samples.

Sample	1	2	3	4	5
Dry density, ρ_{0d} (g/cm^3)	1.730	1.730	1.730	1.730	1.730
Wet density, ρ_0 (g/cm^3)	1.730	1.730	1.911	1.911	2.026
Degree of saturation, S_{0w}	0	0	0.532	0.532	0.874
Water content, w (%)	0	0	10.3	10.3	17.1

Table 3

ARMOR parameters for dry samples.

Behaviour domain	Parameter	Notation	Value
Isotropic	Initial density	ρ_{0d}	1.730 g/cm^3
	Initial compressibility modulus	K_0	200 MPa
	Initial sound speed	c_0	340 m/s
	Elastic pressure limit	P_{EL}	5 MPa
	Initial grain density	ρ_{0g}	2.613 g/cm^3
Deviatoric	Initial shear modulus	G_0	100 MPa
	Transition pressure	P_t	75 MPa
	Maximum ductile yield strength	Y_{max}	1 MPa

Table 4

Summary of planar shock experimental conditions and measured data.

Shot	Sample	Sample thickness (mm)	Impact velocity (m/s)	Condition	Gauge number	Gauge position (mm ± 0.1)	First shock arrival time (μs ± 0.28)	First shock velocity U_1 (m/s)	VISAR first plateau u_p (m/s)
DM1	1	15.09	524	dry	1A	3.88	3.598	1595 ± 59	214.6 ± 2.1
					1B	7.51	6.358		
					1C	11.24	8.078		
					1D	3.88	3.398		
					1E	7.51	5.648		
					1F	11.31	8.208		
					1X	0.04	1.178		
					1Y	-0.08	1.128		
					1Z	0.1	1.288		
DM2	3	14.97	511	53 % saturation	3A	3.85	3.050	2129 ± 83	273.1 ± 2.7
					3B	7.49	4.820		
					3C	11.24	6.570		
					3D	3.79	2.980		
					3E	7.56	4.810		
					3F	11.35	6.280		
					3X	0.03	1.210		
					3Y	-0.02	1.210		
					3Z	-0.03	1.160		
AR1	2	15.08	849	dry	2A	3.78	2.920	2108 ± 85	444 ± 4.4
					2B	7.40	4.498		
					2C	10.26	6.162		
					2D	3.84	3.065		
					2E	7.53	4.646		
					2F	8.99	5.370		
					2X	-0.04	1.073		
					2Y	-0.04	1.274		
					2Z	-0.01	1.117		
AR2	4	15.00	851	53 % saturation	4A	3.77	2.546	2877 ± 129	486.5 ± 4.9
					4B	7.52	3.872		
					4C	11.29	5.104		
					4D	3.70	2.685		
					4E	7.52	3.893		
					4F	11.29	-		
					4X	-0.005	1.088		
					4Y	-0.02	1.534		
					4Z	-0.05	1.126		
AR3	5	15.01	848	87 % saturation	5A	3.80	2.347	3315 ± 139	518.9 ± 5.2
					5B	7.61	3.519		
					5C	11.26	4.594		
					5D	3.86	2.432		
					5E	7.67	3.568		
					5F	11.34	4.545		
					5X	-0.01	1.217		
					5Y	0.04	1.242		
					5Z	0.03	1.090		

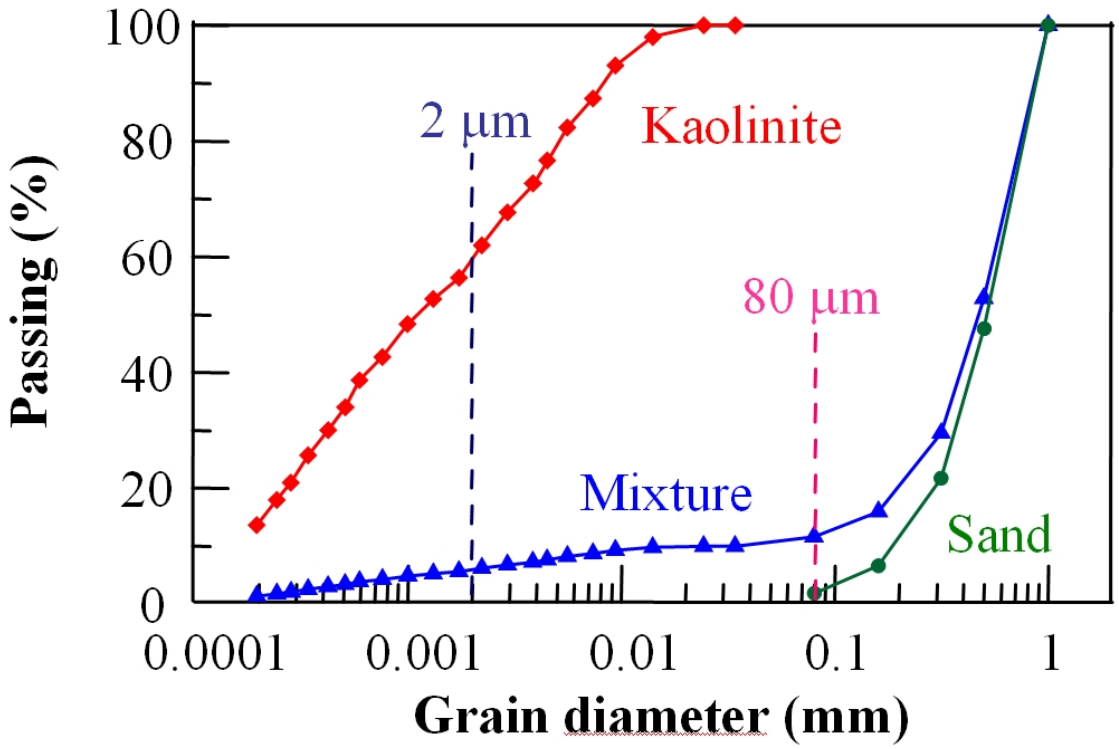
100
80
60
40
20
0
Passing (%)
2 μm
Kaolinite
80 μm
Mixture
Sand
0.0001
0.001
0.01
0.1
1
Grain diameter (mm)

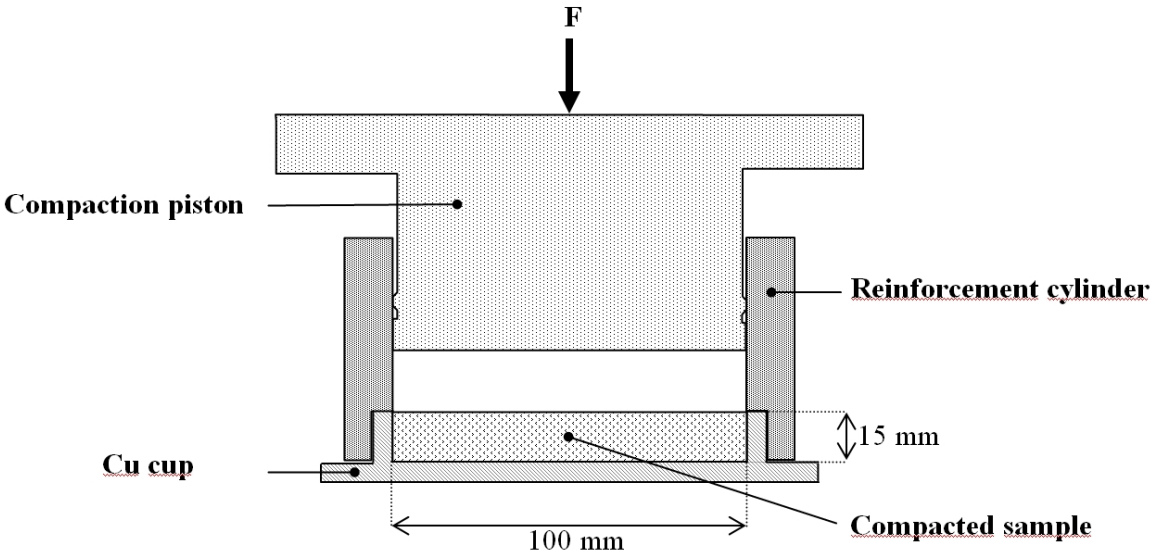

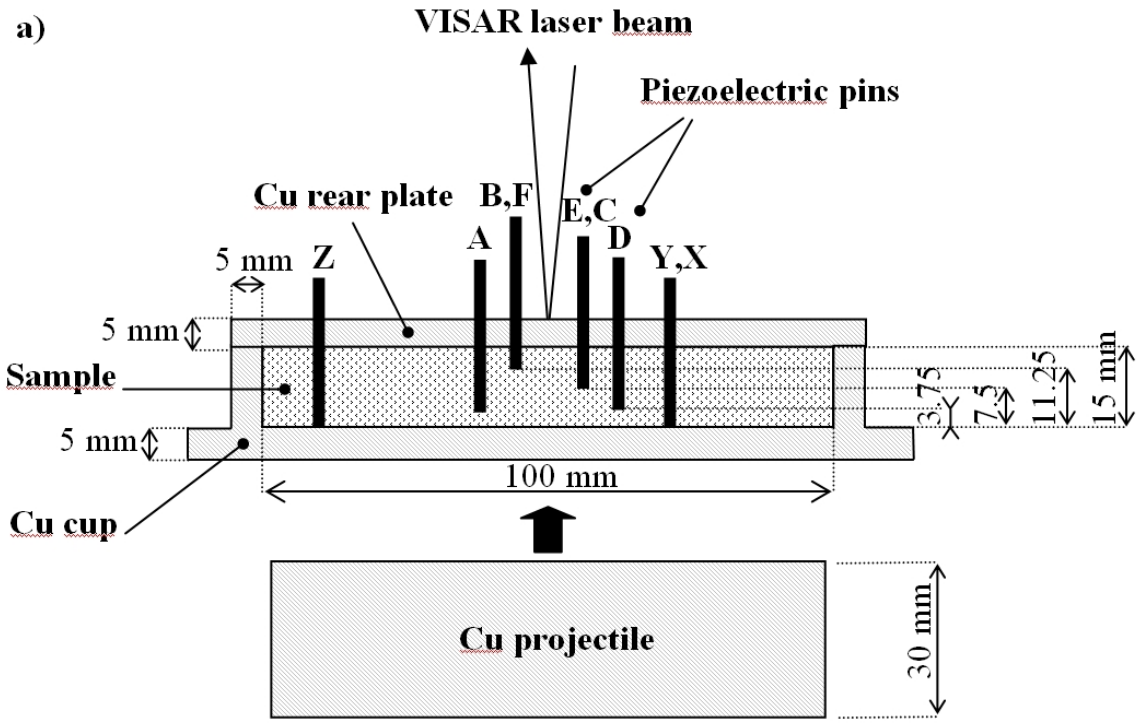
a)
VISAR laser beam
Piezoelectric pins
Cu rear plate
B,F
E,C
A
D
Y,X
Z
5 mm
5 mm
Sample
5 mm
Cu cup
100 mm
3.75
7.5
11.25
15 mm
Cu projectile
30 mm

b)

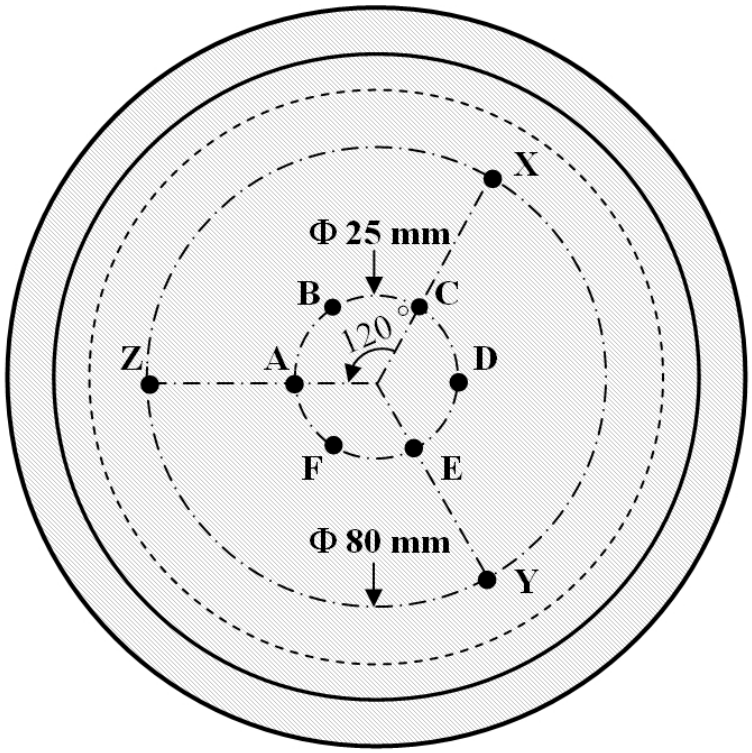

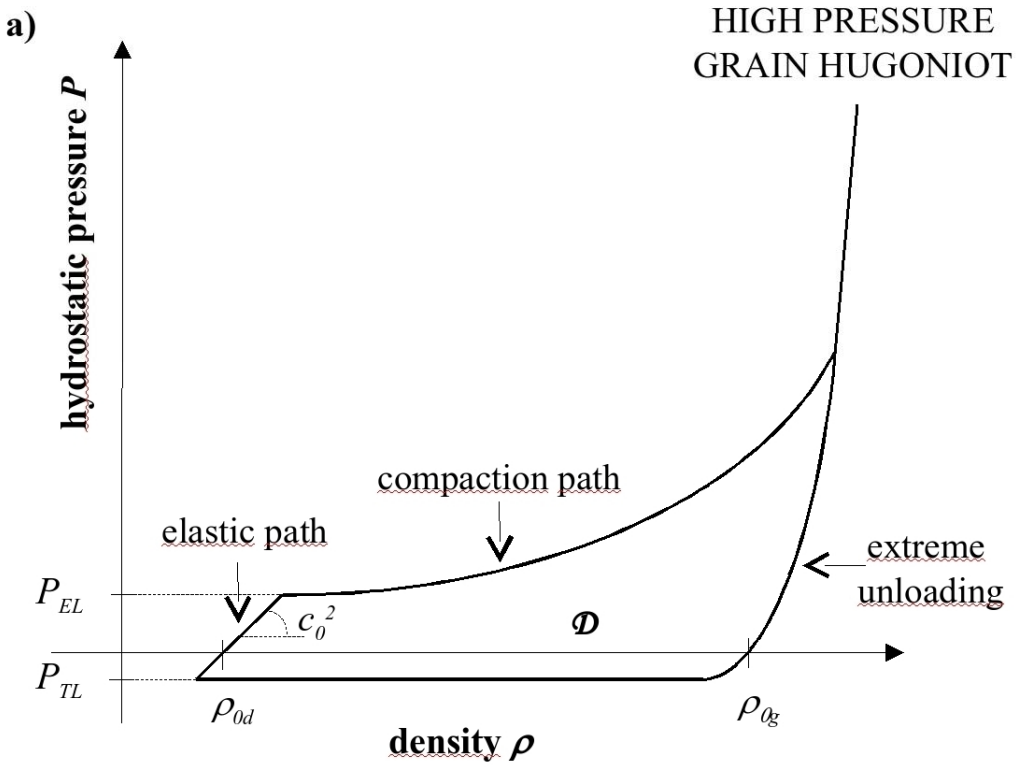
a)
HIGH PRESSURE
GRAIN HUGONIOT
hydrostatic pressure P
compaction path
elastic path
extreme
unloading
P_{EL}
P_{TL}
c_0^2
$\mathcal{D}$
ρ_{0d}
ρ_{0g}
density ρ

b)

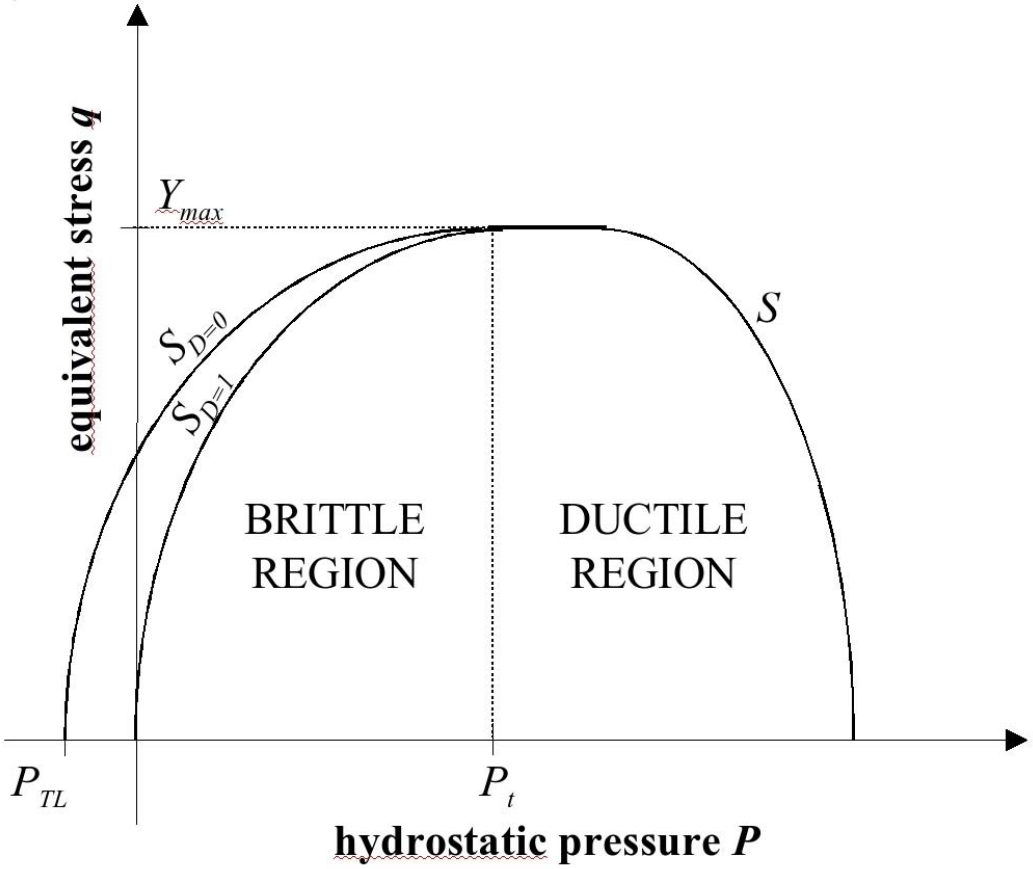
equivalent stress q
Y_{max}
$S_{D=0}$
$S_{D=1}$
S
BRITTLE REGION
DUCTILE REGION
P_{TL}
P_t
hydrostatic pressure P

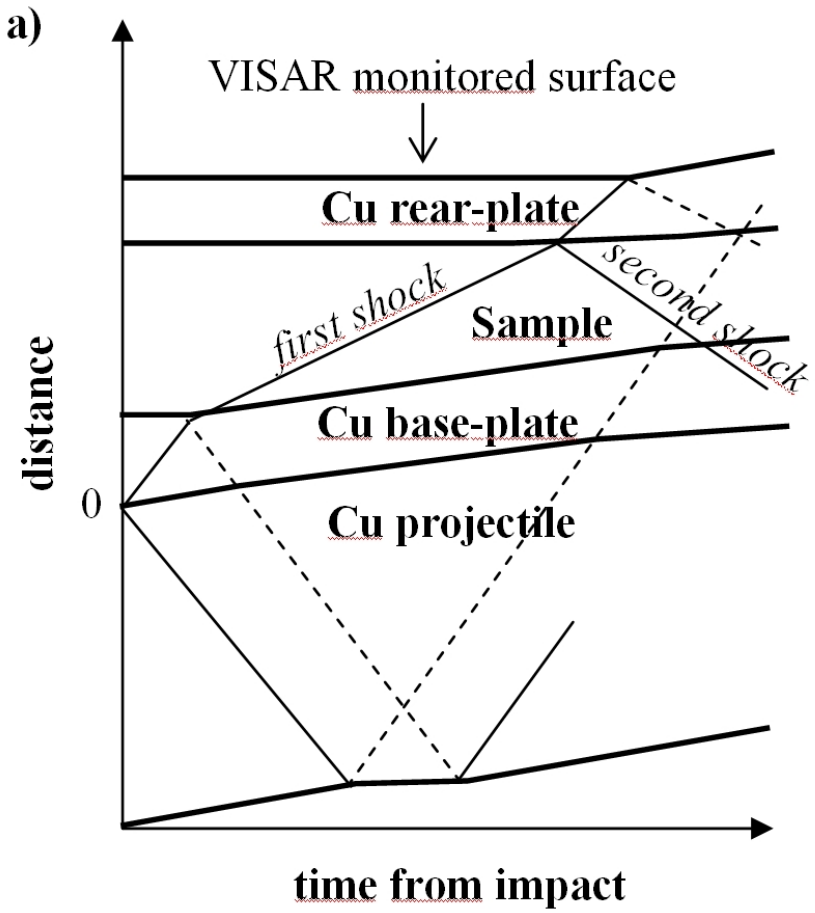
a)
VISAR monitored surface
Cu rear-plate
first shock
second shock
Sample
Cu base-plate
Cu projectile
distance
0
time from impact

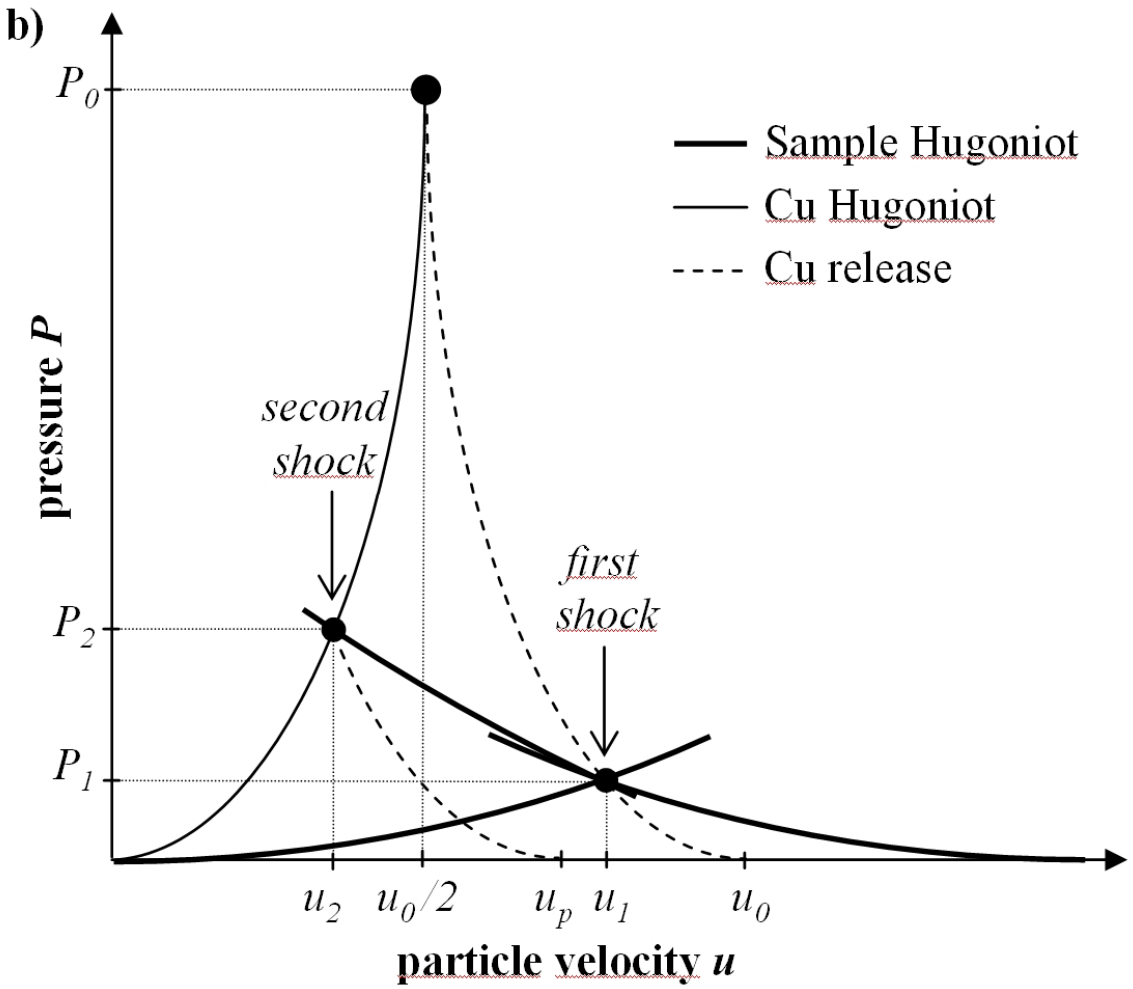
b)
P_0
P_2
P_1
pressure P
Sample Hugoniot
Cu Hugoniot
Cu release
second shock
first shock
u_2
$u_0/2$
u_p
u_1
u_0
particle velocity u

a)

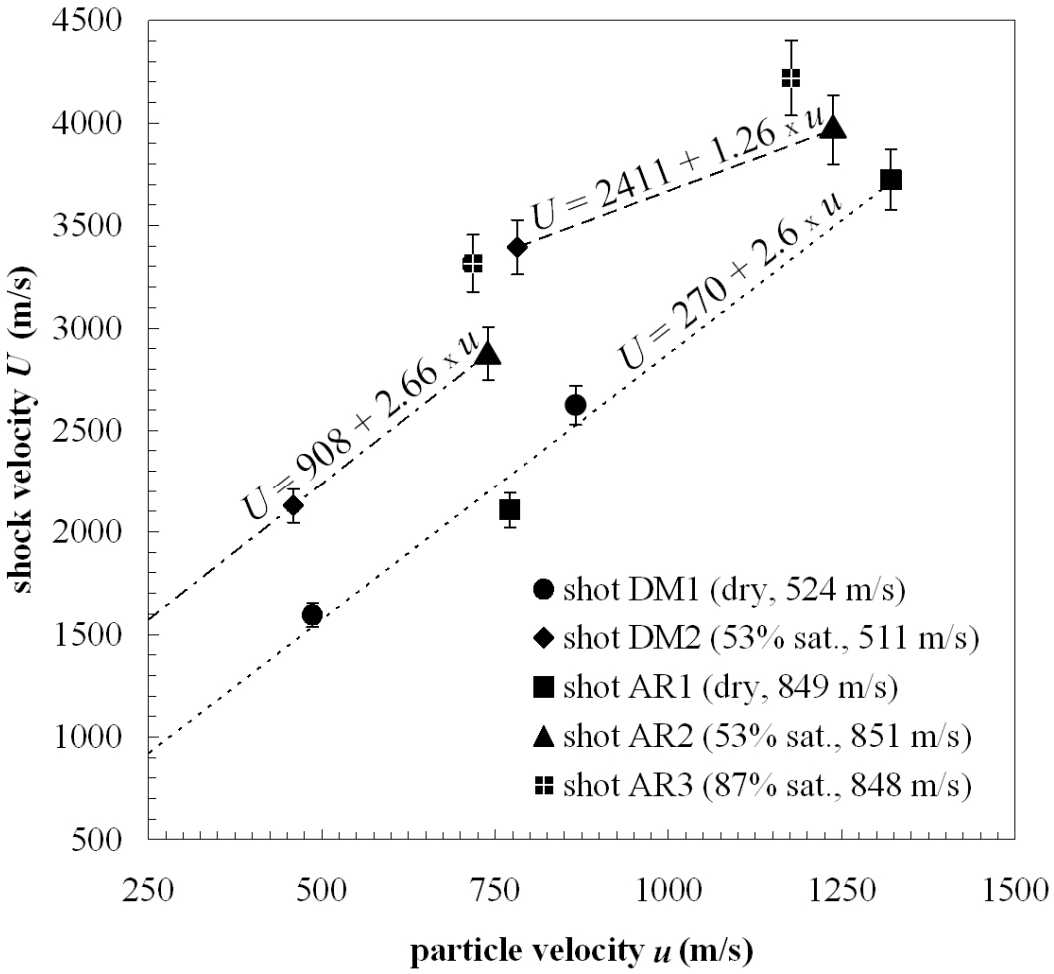
4500
4000
3500
3000
2500
2000
1500
1000
500
250
500
750
1000
1250
1500
shock velocity U (m/s)
particle velocity u (m/s)
U = 2411 + 1.26 x u
U = 908 + 2.66 x u
U = 270 + 2.6 x u
shot DM1 (dry, 524 m/s)
shot DM2 (53% sat., 511 m/s)
shot AR1 (dry, 849 m/s)
shot AR2 (53% sat., 851 m/s)
shot AR3 (87% sat., 848 m/s)

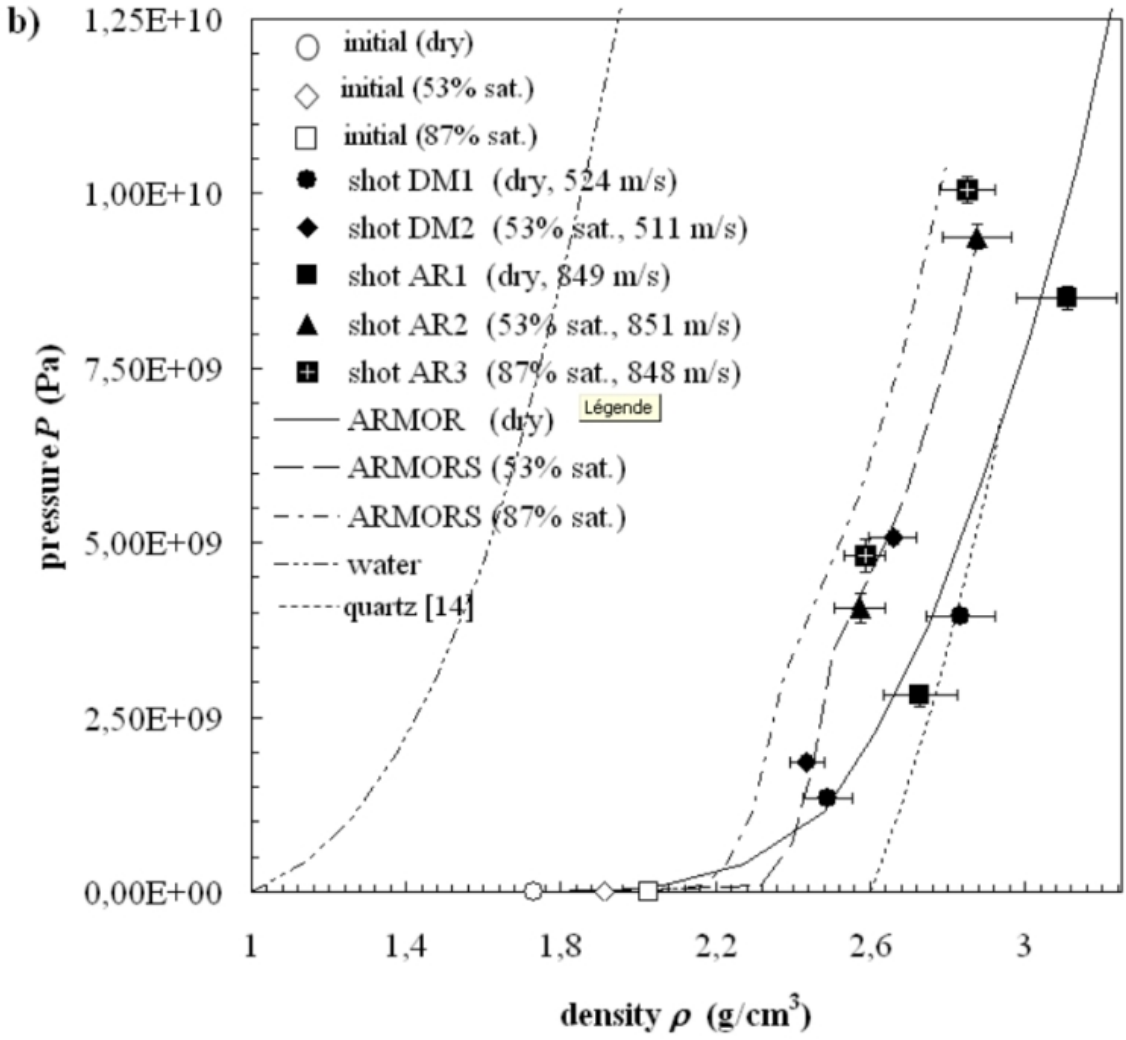
b)
1,25E+10
1,00E+10
7,50E+09
5,00E+09
2,50E+09
0,00E+00
pressure P (Pa)
initial (dry)
initial (53% sat.)
initial (87% sat.)
shot DM1 (dry, 524 m/s)
shot DM2 (53% sat., 511 m/s)
shot AR1 (dry, 849 m/s)
shot AR2 (53% sat., 851 m/s)
shot AR3 (87% sat., 848 m/s)
Légende
ARMOR (dry)
ARMORS (53% sat.)
ARMORS (87% sat.)
water
quartz [14]
1
1,4
1,8
2,2
2,6
3
density ρ (g/cm3)

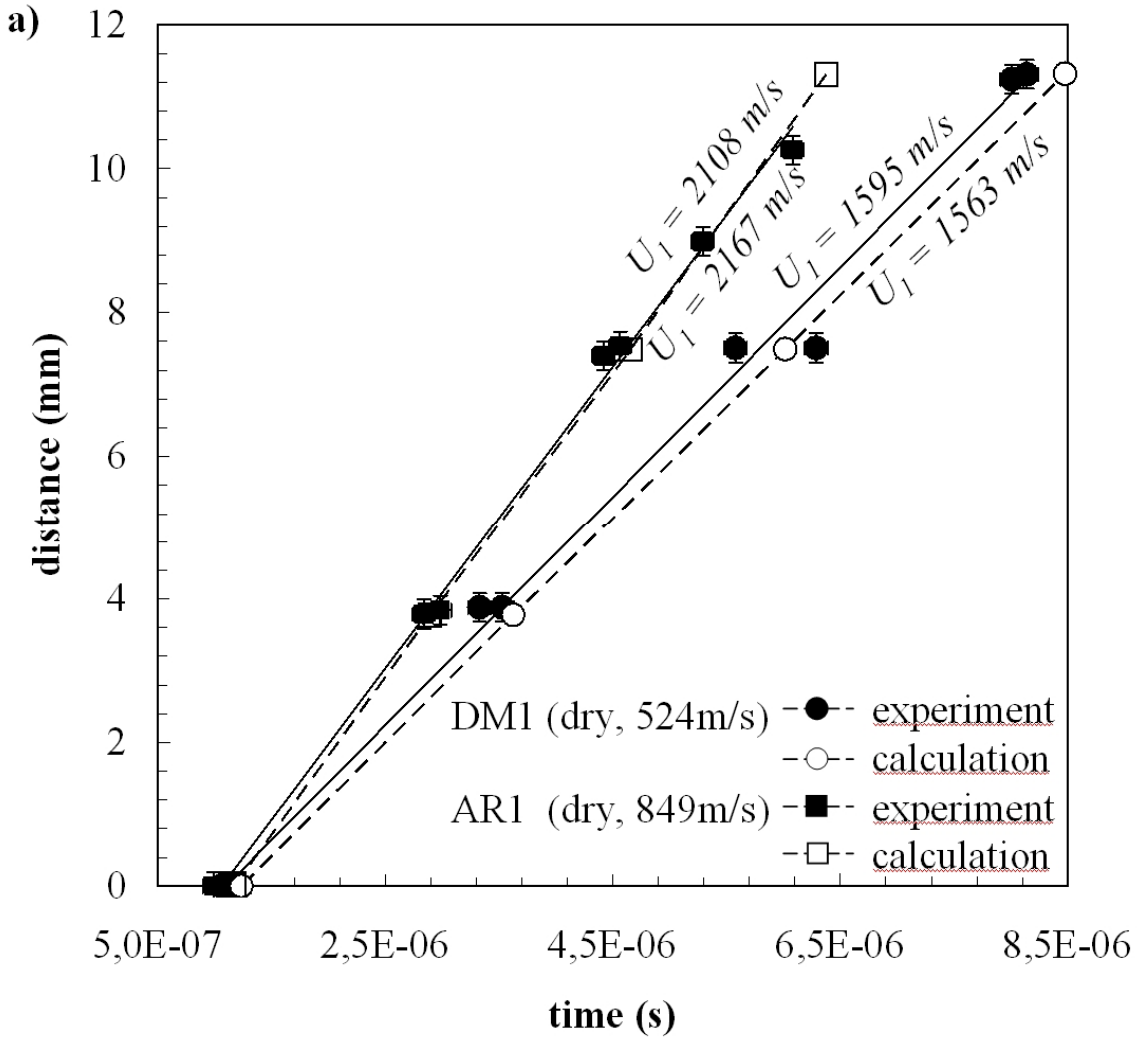
a)
12
10
8
6
4
2
0
distance (mm)
5,0E-07
2,5E-06
4,5E-06
6,5E-06
8,5E-06
time (s)
U1 = 2108 m/s
U1 = 2167 m/s
U1 = 1595 m/s
U1 = 1563 m/s
DM1 (dry, 524m/s)
experiment
calculation
AR1 (dry, 849m/s)
experiment
calculation

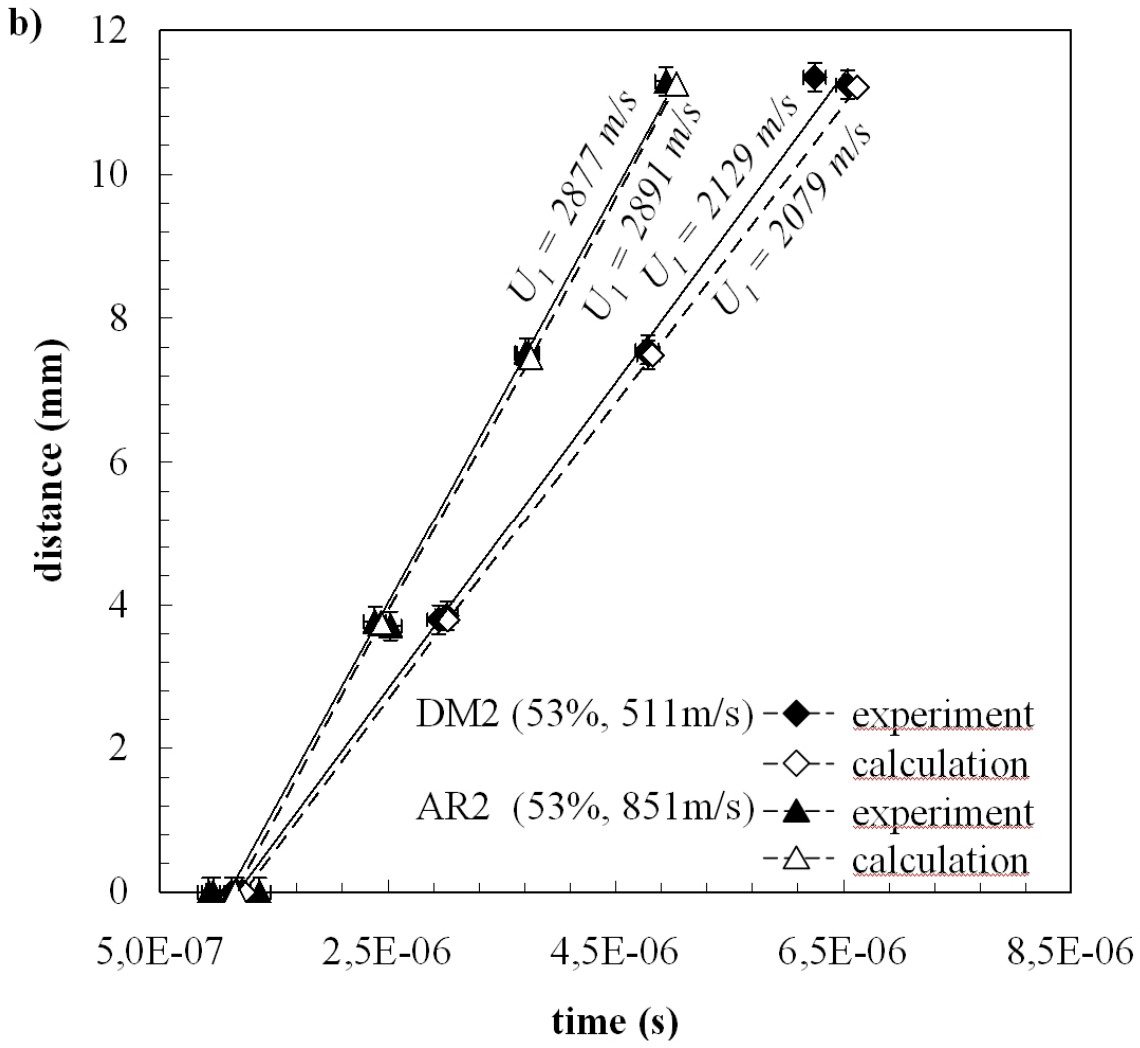
b)
12
10
8
6
4
2
0
distance (mm)
5,0E-07
2,5E-06
4,5E-06
6,5E-06
8,5E-06
time (s)
U1 = 2877 m/s
U1 = 2891 m/s
U1 = 2129 m/s
U1 = 2079 m/s
DM2 (53%, 511m/s) experiment
calculation
AR2 (53%, 851m/s) experiment
calculation

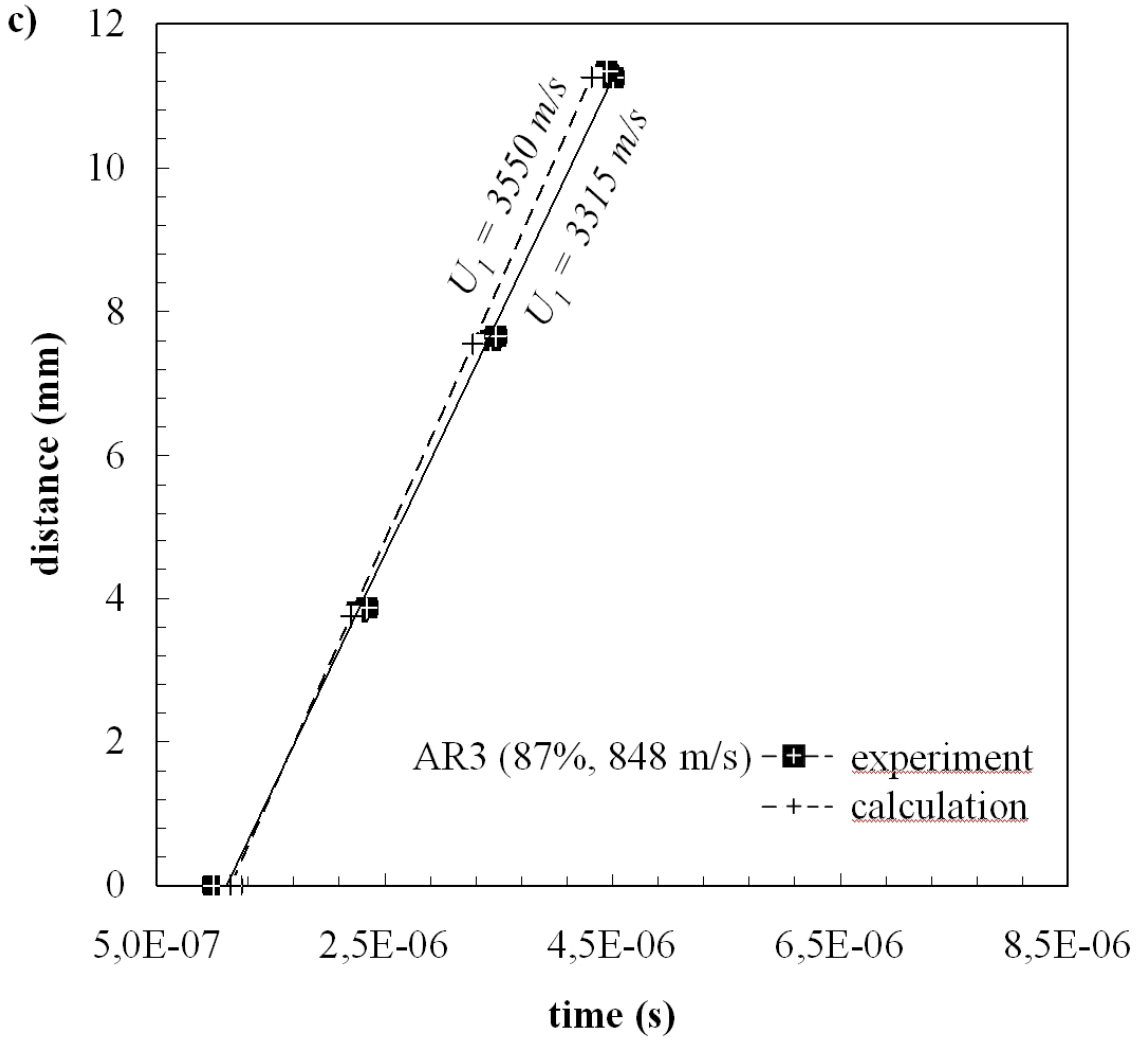
c)
12
10
8
6
4
2
0
distance (mm)
U_1 = 3550 m/s
U_1 = 3315 m/s
AR3 (87%, 848 m/s)
experiment
calculation
5,0E-07
2,5E-06
4,5E-06
6,5E-06
8,5E-06
time (s)

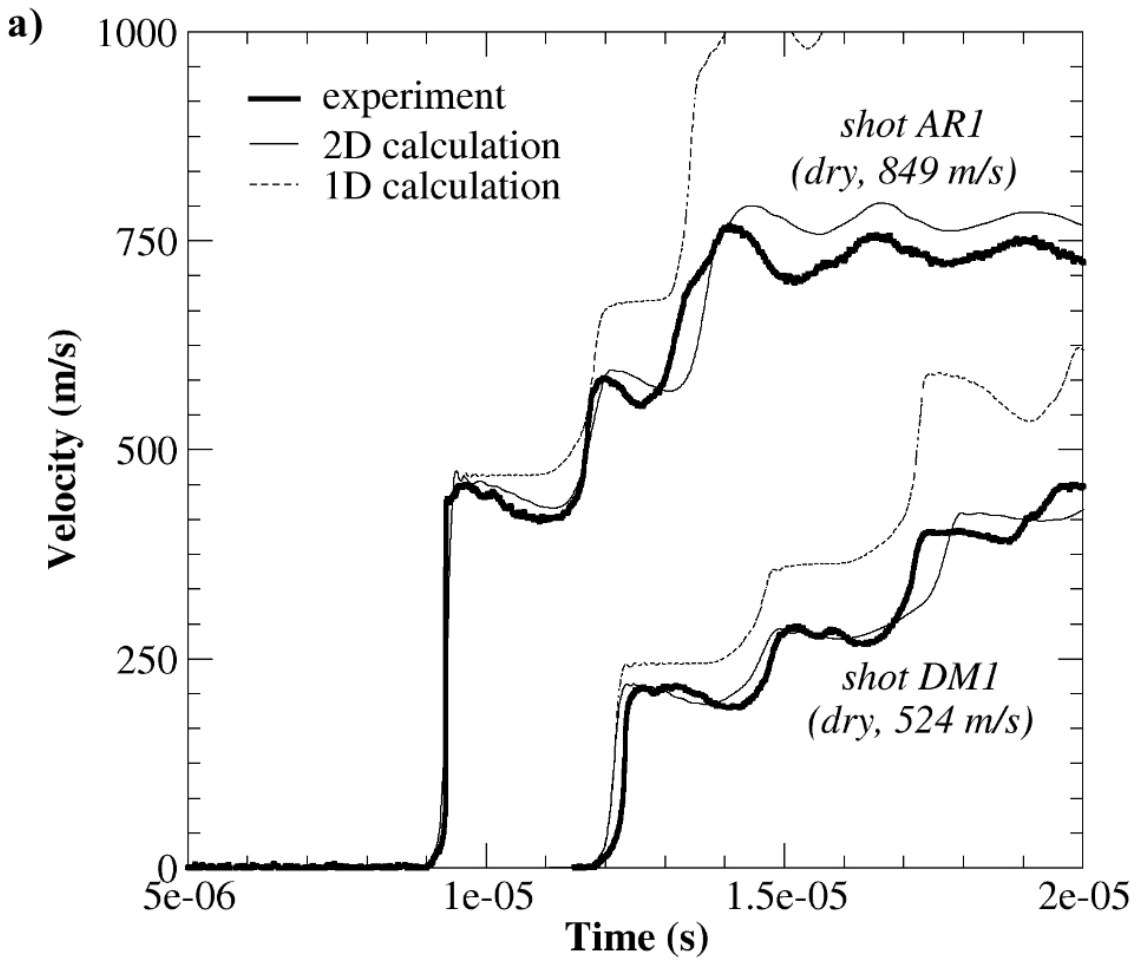
a)
1000
750
500
250
0
Velocity (m/s)
experiment
2D calculation
1D calculation
shot AR1
(dry, 849 m/s)
shot DM1
(dry, 524 m/s)
5e-06
1e-05
1.5e-05
2e-05
Time (s)

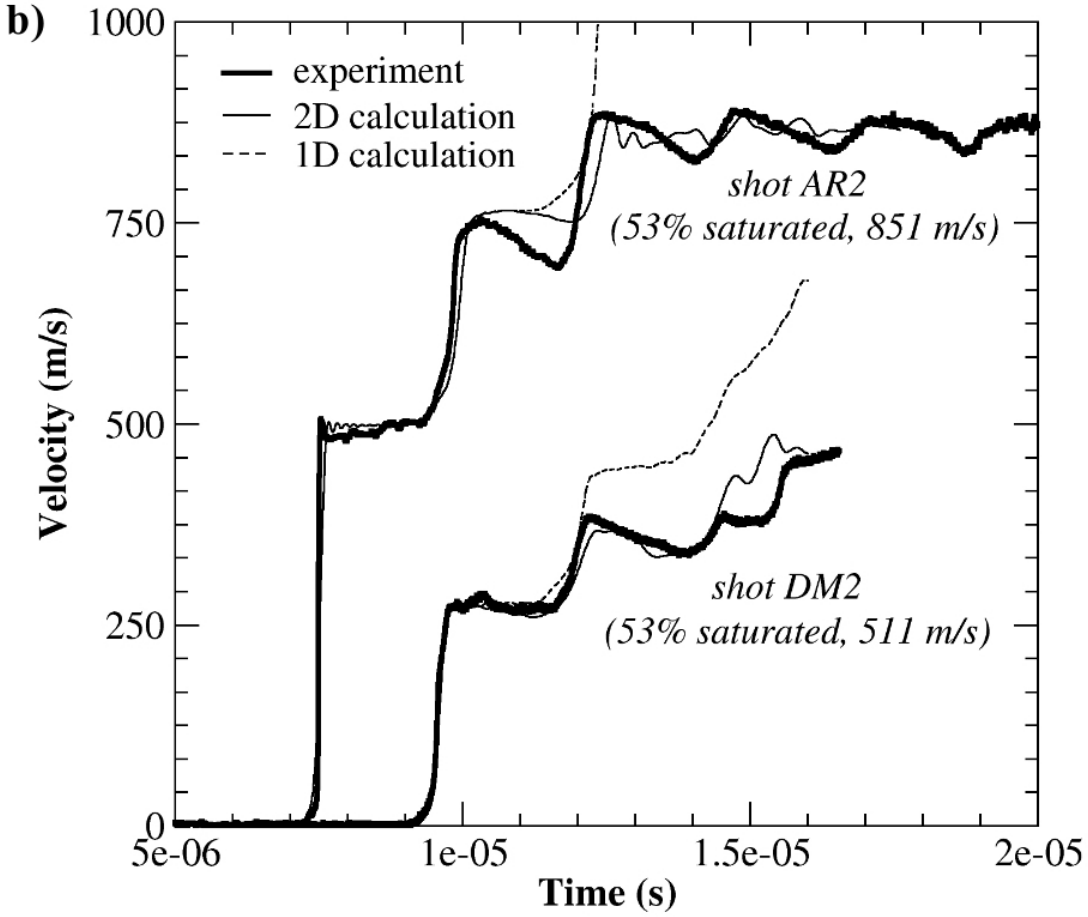
b)
1000
750
500
250
0
Velocity (m/s)
experiment
2D calculation
1D calculation
shot AR2
(53% saturated, 851 m/s)
shot DM2
(53% saturated, 511 m/s)
5e-06
1e-05
1.5e-05
2e-05
Time (s)

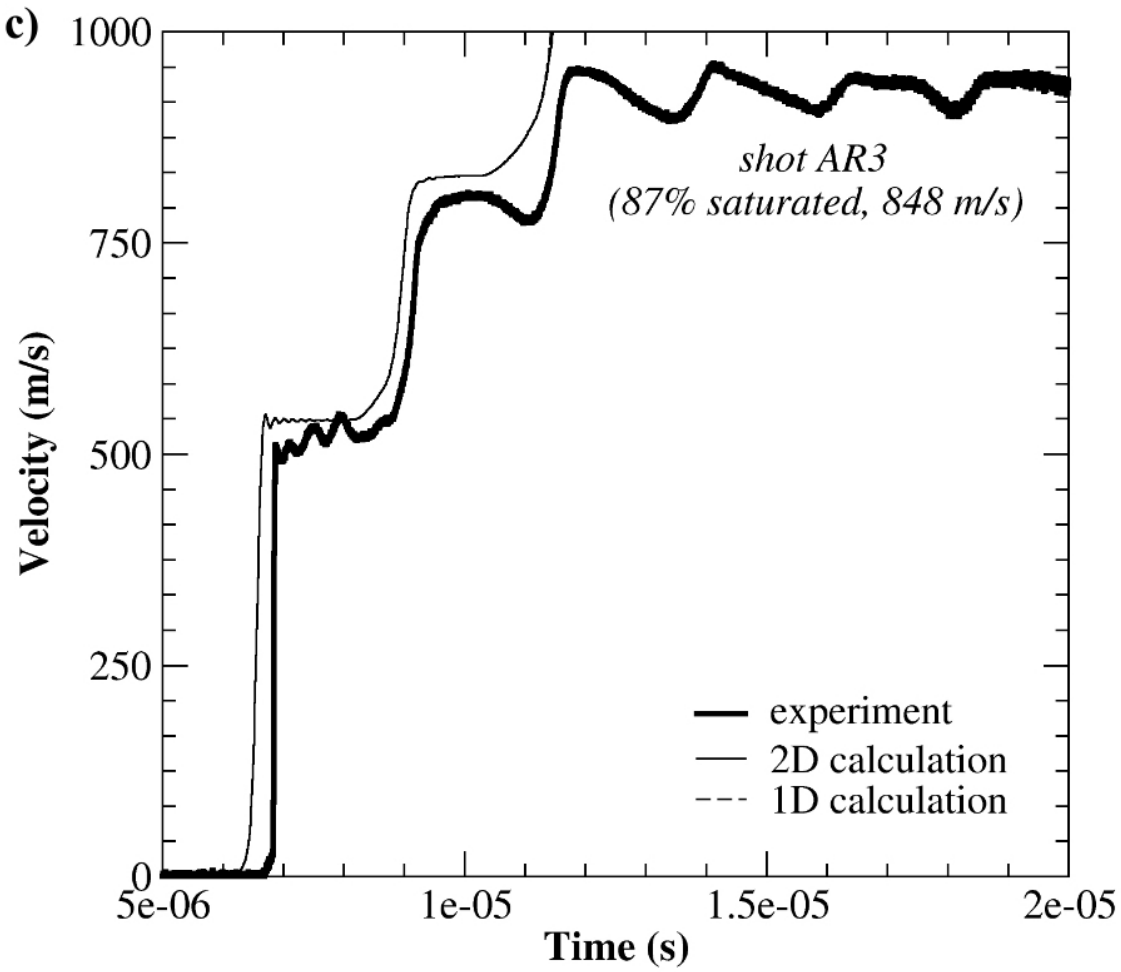
c)
1000
750
500
250
0
Velocity (m/s)
shot AR3
(87% saturated, 848 m/s)
experiment
2D calculation
1D calculation
5e-06
1e-05
1.5e-05
2e-05
Time (s)